Mon. Not. R. Astron. Soc. **342,** 134–144 (2003)

The high-energy polarization-limiting radius of neutron star magnetospheres – I. Slowly rotating neutron stars

Jeremy S. Heyl,[1]★† Nir J. Shaviv[2]‡ and Don Lloyd[1]

[1]*Harvard College Observatory, MS-51, 60 Garden Street, Cambridge, MA 02138, USA*
[2]*Canadian Institute for Theoretical Astrophysics, University of Toronto, 60 St George Street, Toronto, Ontario, Canada M5S 3H8*

Accepted 2003 February 11. Received 2003 February 6; in original form 2001 May 21

ABSTRACT

In the presence of strong magnetic fields, the vacuum becomes a birefringent medium. We show that this quantum electrodynamics effect decouples the polarization modes of photons leaving the neutron star (NS) surface. Both the total intensity and the intensity in each of the two modes are preserved along the path of a ray through the NS magnetosphere. We analyse the consequences that this effect has on aligning the observed polarization vectors across the image of the stellar surface to generate large net polarizations. In contrast to previous predictions, we show that the thermal radiation of NSs should be highly polarized even in the optical. When detected, this polarization will be the first demonstration of vacuum birefringence. It could be used as a tool to prove the high magnetic field nature of anomalous X-ray pulsars (AXPs) and it could also be used to constrain physical NS parameters, such as R/M, to which the net polarization is sensitive.

Key words: polarization – stars: neutron – X-rays: stars.

1 INTRODUCTION

The thermal radiation of isolated neutron stars (NSs) has the potential to teach us much concerning the properties of NSs. Its advantage over non-thermal emission (in radio, optical, X-ray and gamma-ray bands) is that the theory behind the emission is significantly better understood and the radiation actually comes from the surface of the compact object. Because the thermal emission is expected to be intrinsically polarized, more information could potentially be learned by the detection and analysis of polarization measurements. Recent observations with the *ROSAT*, *ASCA*, *Chandra* and *XMM–Newton* missions have shown that some of these sources are bright enough to be potential candidates for X-ray polarimetry in future missions. Moreover, the thermal radiation of some of the isolated NSs can even be detected at optical wavelengths. Thus, it is worthwhile understanding how this polarization is generated and conserved, and what additional information can actually be extracted from its measurement.

In the presence of strong magnetic fields, the opacity of ionized matter to the transfer of photons becomes polarization dependent (Lodenqual et al. 1974; Ventura 1979). This is chiefly because it is easier to scatter electrons in the direction along the magnetic field than it is in a perpendicular direction. Thus, the opacity of light rays with their electric vector polarized perpendicular to the magnetic field would be significantly reduced. A typical photon with this polarization is emitted or scattered last deeper in the atmosphere than one in the other mode. The deeper regions of the atmosphere are hotter, so more flux emerges in this polarization state. Nearly complete polarization can result for the thermal emission (Kanno 1975; Pavlov & Shibanov 1978; Ventura, Nagel & Meszaros 1979).

An observer will see photons originating from the entire surface of the NS hemisphere facing her. Thus, the different polarizations should be added together appropriately. If nothing happens to the photons and their polarization as they propagate from the NS surface, then the polarizations observed at infinity can be added rather simply, as was performed by Kanno (1975) in a simple model for the atmosphere. Pavlov & Zavlin (2000) used a more realistic atmosphere and calculated the net observed polarization while taking the effects that general relativity (GR) has on the magnetic field and on light ray bending. In both cases, net polarizations of the order of 5–30 per cent are obtained because the polarizations of the radiation arriving from different regions of the surface tend to cancel each other.

The above analyses, however, did not consider the effects of quantum electrodynamics- (QED-) induced vacuum birefringence. When QED is coupled to strong magnetic fields, several interesting consequences are obtained. For example, it was shown by Pavlov & Shibanov (1978) and Meszaros & Ventura (1979) that QED has to be taken into account when calculating the appropriate opacity, especially near the cyclotron resonance. This is the case even though a priori it appears that the plasma effects should dominate. More relevant to us is the fact that QED turns the vacuum into a

★E-mail: jheyl@cfa.harvard.edu
†Chandra Postdoctoral Fellow.
‡Current address: Racah Institute of Physics, Hebrew University, Jerusalem 91904, Israel.

birefringent medium when strong magnetic fields are present (Tsai & Erber 1975; Heyl & Hernquist 1997).

In a series of recent papers, we have examined several consequences of vacuum birefringence in neutron-star magnetospheres. When the fields are significantly stronger than the critical QED field of $B_{\rm QED} = 4.4 \times 10^{13}$ G, then the index of refraction of one polarization state can be significantly different from unity and magnetic lensing can result (Shaviv, Heyl & Lithwick 1999). The main result of this lensing effect is that the effective surface area of the NS as measured by the two polarization states is different.

When weaker fields are present, the birefringence can still have interesting implications. At a particular frequency, the vacuum will only decouple the polarization modes out to a particular distance from the surface of the star. Up to this radius, radiation polarized perpendicular to the magnetic field will remain perpendicular to the local direction of the magnetic field even if the direction of the field changes along the path. If the modes only begin to mix at a significant fraction of the distance to the light cylinder, even if the intrinsic polarization at the surface is constant over energy, photons of different energies will exhibit different directions of polarization after passing through the magnetosphere (Heyl & Shaviv 2000) and a circular component of the polarization will develop. Similar effects arise at lower frequencies, when plasma birefringence is considered (Cheng & Ruderman 1979; Barnard 1986).

In Heyl & Shaviv (2002), we showed that QED birefringence is also important for the polarization evolution close to the NS. When it is properly taken into account, a very large net polarization should be observed. This is counter to previous predictions (e.g. Pavlov & Zavlin 2000). As a result, larger polarization signals will be observable, which will allow more information to be extracted from the observation of the thermal radiation. Measurement of the high polarization will also serve as the first direct evidence of the birefringence of the magnetized vacuum arising from QED and a direct probe of the behaviour of the vacuum at magnetic fields of the order of and above the critical QED field of $B_{\rm QED} = 4.4 \times 10^{13}$ G. This should be contrasted with the decades of Earth-based experiments that have not succeeded thus far in detecting the vacuum birefringence induced by strong magnetic fields (Iacoponi & Zavattini 1979; Bakalov et al. 1998; Rizzo 1998; Nezrick 1999).

We begin in Section 2 with the description of the physics needed to calculate the polarization to be observed at infinity. In Section 3, we elaborate the results presented in Heyl & Shaviv (2002) and build upon them to understand the observational signatures of vacuum polarization in rotating neutron stars. Section 3.3.2 estimates the strength of the polarized signal averaged over the rotation of the star for the subset of radio pulsars for which we know the geometry of the dipole field. We end in Section 4 with a discussion of the ramifications of this effect.

2 CALCULATIONS

Several ingredients are needed for the calculation of the net polarization to be observed at infinity. First, the structure of the magnetic field must be specified. We assume that the magnetic field is a centred dipole. Secondly, we need a model for the intrinsic polarization emitted by a magnetized atmosphere. For simplicity, we assume here that the atmospheres emit completely (linearly) polarized radiation. In a large frequency range, it is more than an adequate approximation because the effective temperature for the two polarizations will be markedly different if high magnetic fields are present. For example, at photon energies E_γ much below the electron rest energy and cyclotron energy $E_{\rm cyc,e}$, but much above the ion cyclotron energy, the typical degree of linear polarization $p_{\rm L}$ should be $1 - p_{\rm L} \sim \mathcal{O}(E_\gamma / E_{\rm cyc,e})^2$, unless the angle between the magnetic field $\boldsymbol{B}$ and the photon wavevector $\boldsymbol{k}$ is very small (Pavlov & Zavlin 2000).

To calculate the observed polarization at infinity, we need to calculate the trajectories of the light rays, which are bent owing to GR. Along these trajectories, we have to solve for the evolution of the polarization. This will be dominated by the vacuum birefringence.

2.1 Photon trajectories

In calculating the trajectories of the photons we assume that the field is sufficiently weak such that the refractive index for both modes is approximately unity throughout the magnetosphere (cf. Shaviv et al. 1999). We also neglect the effect of the rotation of the star on the space–time surrounding it.

Without rotation, all planes that pass through the centre of the star are equivalent, so we can integrate the equations of motion for a photon in the equatorial plane of the Schwarzschild metric. The trajectory is determined uniquely by the impact parameter b. To integrate the polarization, we require the position of the photon as a function of the proper length along its path. Misner, Thorne & Wheeler (1973) give the differential equations for the trajectory

$$\frac{{\rm d}t}{{\rm d}\lambda} = \left(1 - \frac{2M}{r}\right)^{-1} \tag{1}$$

$$\frac{{\rm d}r}{{\rm d}\lambda} = \left[1 - \frac{b^2}{r^2}\left(1 - \frac{2M}{r}\right)\right]^{1/2} \tag{2}$$

$$\frac{{\rm d}\theta}{{\rm d}\lambda} = 0 \tag{3}$$

$$\frac{{\rm d}\phi}{{\rm d}\lambda} = \frac{b}{r^2}, \tag{4}$$

and also

$$\frac{{\rm d}l}{{\rm d}\lambda} = \left(1 - \frac{2M}{r}\right)^{-1/2}, \tag{5}$$

where M is the gravitational mass of the star. Combining equations (2) and (4) yields a separable equation for $\phi(r)$, which is useful for quickly determining to which part of the star a region of the image corresponds (Page 1995),

$$\phi - \phi_0 = x \int_0^{M/R} \left[\left(1 - \frac{2M}{R}\right)\left(\frac{M}{R}\right)^2 - (1 - 2u)\, u^2 x^2\right]^{-1/2} {\rm d}u, \tag{6}$$

where $x \equiv b/R_\infty$ and $R_\infty \equiv R\,(1 - 2M/R)^{-1/2}$, with R being the circumferential radius of the star.

2.2 Polarization trajectories

The polarization lies in the plane perpendicular to the trajectory of the photon. Unlike in flat space–time, because the photon travels along a curved path, the orientation of this plane with respect to a distant observer necessarily varies along the path. Under the assumption that the space surrounding the neutron star is devoid of material and non-gravitational fields, the polarization is constant, if it is defined in a basis consisting of a vector in the plane of the trajectory and one perpendicular to that plane (Pineault 1977).

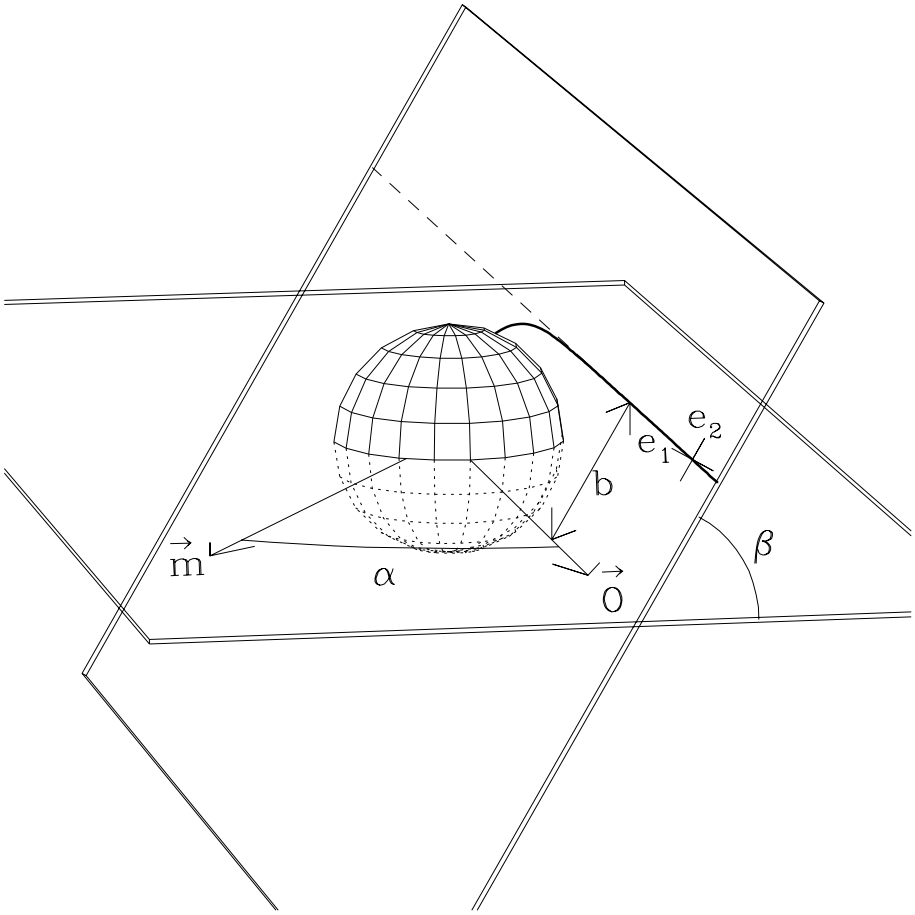

Figure 1. The geometry of the photon trajectory and the polarization basis.

To include the standard general relativistic result naturally, we calculate the evolution of the polarization owing to the birefringence of the vacuum in the aforementioned basis. Fig. 1 shows an example trajectory along with the polarization basis at a particular point. α is the angle between the magnetic dipole ($\boldsymbol{m}$) and the line of sight ($\boldsymbol{O}$), and β is the angle between the trajectory plane and the $\boldsymbol{m}$–$\boldsymbol{O}$ plane.

Kubo & Nagata (1983) find that the evolution of the polarization of a wave travelling through a birefringent and dichroic medium in the limit of geometrical optics is given by

$$\frac{\partial \boldsymbol{s}}{\partial l} = \hat{\boldsymbol{\Omega}} \times \boldsymbol{s} + (\hat{\boldsymbol{T}} \times \boldsymbol{s}) \times \boldsymbol{s}, \tag{7}$$

where l is the proper distance along the trajectory, $\boldsymbol{s}$ is the normalized Stokes vector (Jackson 1975), and $\hat{\boldsymbol{\Omega}}$ and $\hat{\boldsymbol{T}}$ are the birefringent and dichroic vectors. The Stokes vector consists of the four Stokes parameters, S_0, S_1, S_2 and S_3. The vector $\boldsymbol{s}$ consists of S_1/S_0, S_2/S_0 and S_3/S_0. The result was found by Kubo & Nagata (1983) for any dielectric medium and it was extended for a medium that is both dielectric and permeable by Heyl & Shaviv (2000).

As Heyl & Shaviv (2000) argue, QED decouples the polarization states in the vacuum for sufficiently strong fields. Here we will restrict ourselves to fields substantially less than $B_{\rm QED} \approx 4.4 \times 10^{13}$ G. A field of 10^{12} G is sufficient to decouple the polarization states at the surface of a neutron star for $\nu \gtrsim 10^{12}$ Hz. A plasma with the Goldreich–Julian density decouples the polarization states of photons with $\nu \lesssim 10^{14}$ Hz. Here we will focus on ultraviolet (UV) to X-ray radiation, so the plasma contribution to the index of refraction may be neglected. We will consider photons with $\nu \lessapprox 10^{14}$ Hz (i.e. for which the plasma would be important), but we will also neglect the plasma contribution so we can connect our results with those of Pavlov & Zavlin (2000) who neglect the birefringence of the magnetosphere entirely.

If one neglects the plasma and takes the weak-field limit, the dichroic vector vanishes and the magnitude of the birefringent vector is

$$\left|\hat{\boldsymbol{\Omega}}\right| = \frac{2}{15}\frac{\alpha_{\rm QED}}{4\pi}\frac{\omega}{c}\left(\frac{B_\perp}{B_{\rm QED}}\right)^2, \tag{8}$$

and it points in the direction of the projection of the magnetic field on to the Poincaré sphere. $B_\perp$ is the strength of the magnetic field perpendicular to the direction of the propagation of the photon. We assume that the magnetic field is a centred dipole and we neglect the distortion of the magnetic field as a result of general relativity. For the masses and radii that we are considering, the perturbation to the field strength is at most a factor of 2 and the change in the direction of the field is less than 5° throughout (Ginzburg & Ozernoĭ 1965). Both the value of the polarization-limiting radius and the emergent flux depend weakly on the strength of the magnetic field at the surface – both increase as $B^{0.4}$; therefore, this simplification does not have an important effect on the results.

Heyl & Shaviv (2000) find that the polarization states are decoupled as long as the gradient of the index of refraction is not too large,

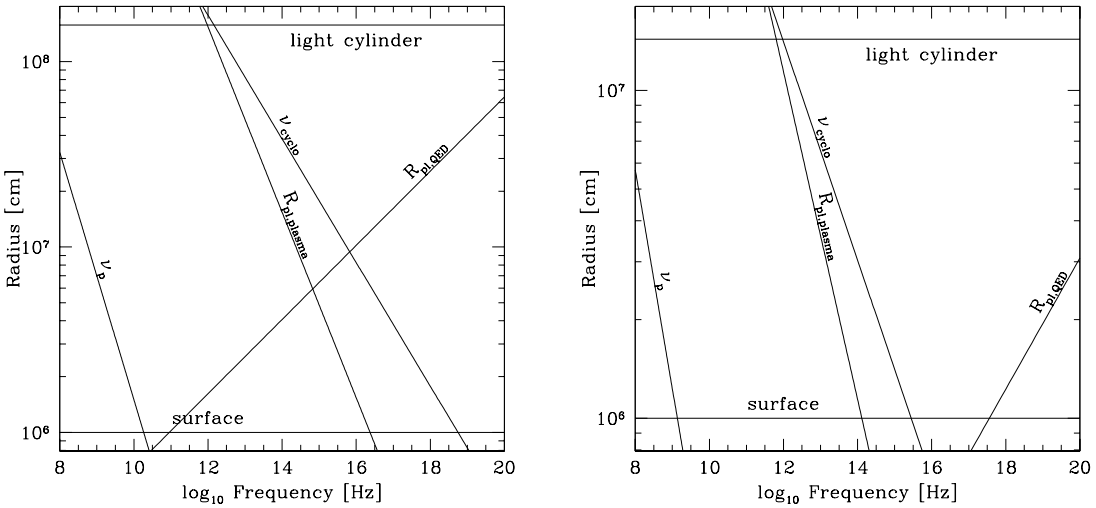

Figure 2. Polarization-limiting radius as a function of frequency. The left-hand panel is for a neutron star with $B = 2 \times 10^{12}$ G and $P = 33$ ms. The right-hand panel is for $B = 10^9$ G and $P = 3$ ms.

specifically

$$\left| \hat{\mathbf{\Omega}} \left(\frac{1}{|\hat{\mathbf{\Omega}}|} \frac{\partial |\hat{\mathbf{\Omega}}|}{\partial l} \right)^{-1} \right| \gtrsim 0.5. \tag{9}$$

For radial trajectories this yields

$$r \lesssim r_{\rm pl} \equiv \left(\frac{\alpha_{\rm QED}}{45} \frac{\nu}{c} \right)^{1/5} \left(\frac{\mu}{B_{\rm QED}} \sin\alpha \right)^{2/5} \approx 1.2 \times 10^7 \mu_{30}^{2/5} \nu_{17}^{1/5} (\sin\alpha)^{2/5} \,{\rm cm}, \tag{10}$$

where μ is the magnetic dipole moment of the star and ν is the frequency of the photon. Also, $\mu_{30} = \mu/(10^{30}$ G cm$^3)$ and $\nu_{17} = \nu/10^{17}$ Hz.

If this condition is not met, the polarization remains constant, i.e. the polarization modes are coupled. Fig. 2 depicts the radii within which either the plasma or the vacuum effectively decouples the polarization modes in the magnetosphere – we have assumed that the plasma density is given by the result of Goldreich & Julian (1969). At distances closer to the star than the polarization-limiting radius ($r_{\rm pl}$), the polarization of the radiation remains in one of the two polarization modes of the strongly magnetized plasma or vacuum.

If the entire surface emits in one polarization mode, i.e. the surface emission is initially fully polarized, the radiation will remain in that mode until the polarization-limiting radius, so one can estimate the observed extent of the polarization geometrically by calculating the solid angle subtended by the image of the surface of the star at the polarization-limiting radius. As the angular size of the image at $r_{\rm pl}$ vanishes, the polarized fraction approaches unity. Numerical integration of the photon paths bears this out.

3 RESULTS

These results assume that $B \ll B_{\rm QED}$ at the decoupling radius. This is always the case for the photon energies of interest, because even if the field on the surface is greater than the QED value, as is the case in magnetars, the decoupling takes place far enough from the surface such that the r^{-3} term will make the field significantly subcritical.

3.1 Effects along a trajectory

We begin by integrating the photon light trajectories for specific photons leaving the NS surface and following the evolution of their polarization. Because the QED vacuum is not dichroic by itself, equation (7) dictates that the amplitude of $\boldsymbol{s}$ does not change along a ray. In the course of evolution, however, the linear component of $\boldsymbol{s}$, i.e. the 1–2 components, may change direction, and the amount of circular component s_3 can change as well. The top part of Fig. 3 depicts the evolution of the angle of $\boldsymbol{s}$ in the 1–2 plane of the Poincaré space, together with the angle of the birefringent vector $\hat{\mathbf{\Omega}}$ (determined by the magnetic field component perpendicular to the ray).

As the particular photon leaves the surface, the magnetic field orientation rotates by approximately 2.2 rad, which corresponds to 4.4 rad in the 1–2 plane of the Poincaré space. Because the coupling is weaker at lower frequencies, the lower-frequency photons follow the direction of the magnetic field up to a smaller distance. Beyond the polarization-limiting distance, the polarization direction freezes. Its direction roughly corresponds to the direction of the magnetic field where the modes couple. Because modes couple gradually, the direction of the magnetic field can change during the coupling process. If the change in direction is rapid, a large circular polarization results. This is seen in the bottom part of Fig. 3. For the low- and high-frequency photons, the coupling takes place before the magnetic field can significantly change or after it has stopped changing, so for these frequencies, the circular component obtained is small. For the intermediate frequency, which for 10^{12} G NSs corresponds to the optical or UV region, the coupling takes place while the direction of the magnetic field is changing and a large circular component is generated.

At high frequencies (hard X-ray to γ-rays), the coupling can take place at a significant fraction of the light cylinder radius. In this case, it was shown by Heyl & Shaviv (2000) that one should take into account the rotation of the NS. Because the modes of higher frequencies couple further from the NS, the directions of the rotating magnetic field at the polarization-limiting radii are different for different photon energies, such that phase leads between different wavebands can result. Because coupling takes place while the NS is rotating, circular polarization can again result.

3.2 The polarization 'image' of an NS

The next step is to construct a polarization 'image' of an NS. The apparent surface is projected on to a surface perpendicular to the

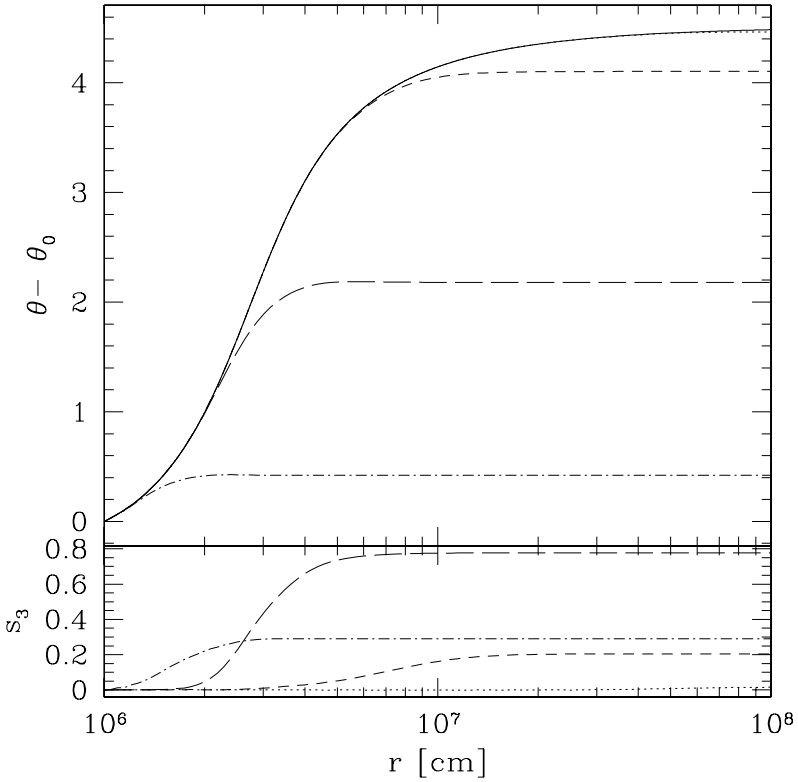

Figure 3. The evolution of the polarization for a particular ray as a function of frequency for $R = 10^6$ cm, $M = 2.1 \times 10^5$ cm, $\alpha = 30^\circ$, $\beta = 148.5^\circ$ and $b = 0.4R_\infty$. The solid curve traces the position angle of the birefringent vector $\hat{\mathbf{\Omega}}$, the dot-dashed line follows the polarization at $\nu\mu_{30}^2 = 10^{21}$ Hz, the long-dashed line at 10^{17} Hz, the short-dashed lines at 10^{15} Hz and the dotted line at 10^{13} Hz.

NS–observer direction. The image is then divided into elements of equal solid angle. Next, light rays are followed from each element of the apparent surface to the observer, taking into account GR light bending (equation 6) and polarization evolution (equation 7), as described in Section 3.1.

Typical results are portrayed in Fig. 4, which shows the polarization observed at infinity overlaying the GR lensed image of the NS. The typical polarization is an ellipse. The major axis describes the direction of the linear polarization (in real space), while the ratio of the minor to major axis gives the amount of circular polarization. Not given in the figure is the sense of rotation of the circular polarization. From symmetry, one obtains that the circular components in the top half of the images are opposite to those in the bottom half. The same is true for the s_2 polarization, which describes the $\pm 45^\circ$ polarization directions in real space. Unlike the s_3 antisymmetry, however, the s_2 antisymmetry is apparent in the images.

The antisymmetry of the s_2 and s_3 components implies that when the polarizations from all the star are added together, only a net s_1 component will result. Namely, the net polarization from the NS will be either in the direction of the magnetic dipole axis or perpendicular to it. This statement will not be true if the cylindrical symmetry is broken, either by the magnetic field, by rotation or by the atmospheric emission.

3.3 The net polarization of an NS

Once a polarization 'image' is calculated, the net polarization seen by an observer is found by integrating the intensity contributed by each of the normal modes of the atmosphere to each of the observed Stokes' parameters. Here we will treat the simple case where the intensity in one mode vanishes ($I_O = 0$) and the intensity in the other mode is isotropic ($I_X =$ constant). In this case, the value of S_1/S_0 is simply the mean value of s_1 evaluated over the observed polarization field (e.g. as depicted in Fig. 4). For this simple model, we denote S_1/S_0 as summed over the entire image by $\bar{s}_1$.

The results for $\bar{s}_1$ as a function of the magnetic field strength and frequency $\nu\mu_{30}^2$ are given in the left-hand panel of Fig. 5, for two inclination angles and three different NS radii: 6, 10 and 18 km. The right-hand panel depicts the net polarization $\bar{s}_1$ as a function of the angle between the line of sight and the magnetic dipole moment for the three NS radii and two frequencies.

Fig. 5 depicts several important trends:

(i) higher-frequency radiation is more strongly polarized;
(ii) more strongly magnetized stars exhibit stronger polarization;
(iii) as the line of sight approaches the direction of the dipole, the net polarization vanishes;
(iv) at high frequencies, the emission from larger stars is *less* polarized; the trend is reversed at low frequencies.

Equation (10) predicts the first three of these trends directly. As the frequency of the photon or the strength of the dipole moment increases, the polarization-limiting radius increases. Also as $\sin\alpha$ increases, the polarization-limiting radius increases. A larger value of $r_{\rm pl}$ results in a larger polarized fraction because the solid angle subtended by the bundle of rays that eventually reach the detector decreases with distance from the star. Over successively smaller solid angles, the magnetic field geometry appears successively more uniform, and the polarization from different regions of the star is added more coherently.

The final trend requires a two-part explanation. If $\nu\mu_{30}^2 \sin^2\alpha \gg 10^{12}$ Hz, then $r_{\rm pl} \gg R$, so the net polarization depends almost entirely on the angular size of the ray bundle. Far from the surface of the

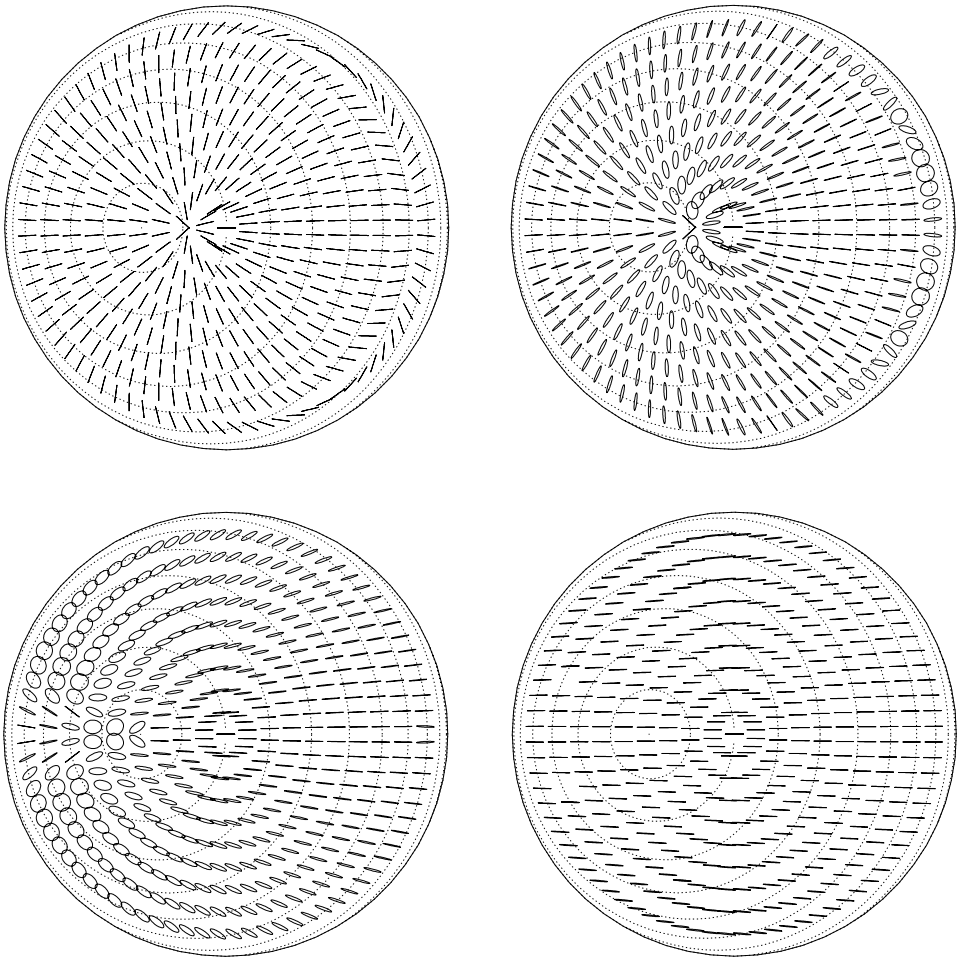

Figure 4. The observed polarization field for $R = 10^6$ cm, $M = 2.1 \times 10^5$ cm and $\alpha = 30^\circ$. The upper left- and right-hand panels are $\nu\mu_{30}^2 = 0$ and 10^{13} Hz, respectively. The lower left- and right-hand panels are $\nu\mu_{30}^2 = 10^{17}$ and 10^{21} Hz, respectively.

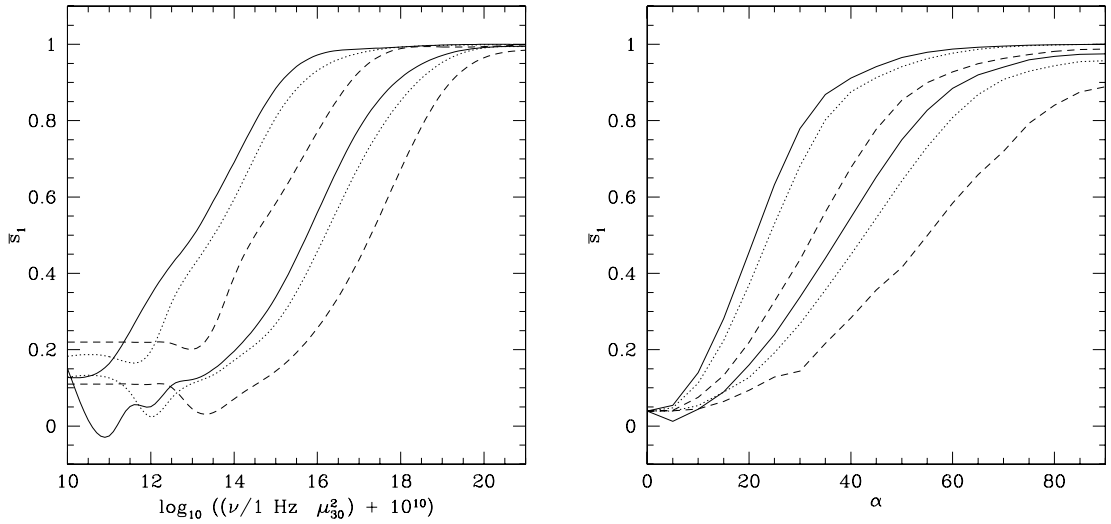

Figure 5. The left-hand panel depicts the polarized fraction as a function of $\nu\mu_{30}^2$ for $R = 6$, 10 and 18 km as solid, dotted and dashed lines, respectively, and $\alpha = 30^\circ$ and 60° for the lower and upper set of curves, respectively. The right-hand panel shows the polarized fraction as a function of α for $R = 6$, 10 and 18 km and $\nu\mu_{30}^2 = 10^{15}$ (lower set) and 10^{17} Hz (upper set).

star, the linear radius of the bundle is $b_{\max}$. For a given mass, $b_{\max}$ decreases with the radius of the star until it reaches a constant value for $R < 3M$; consequently, smaller stars have smaller bundles and larger net polarizations.

For $\nu\mu_{30}^2 \sin^2\alpha \lesssim 10^{12}$ Hz, the polarization-limiting radius is comparable to or smaller than the radius of the star. In this regime, magnetospheric birefringence has little effect on the polarized image; therefore, in this regime, the results of Pavlov & Zavlin (2000)

are obtained. We see a larger fraction of the surface of more compact stars so the net polarization will decrease as M/R increases, because the polarization is then added mostly incoherently. For $R < 3.5M$ we see the entire surface and for $R \leqslant 3M$ we see an infinite number of images of the surface (e.g. Page 1995).

The paragraphs that follow examine the ramifications of these trends in more detail. In particular, we calculate the polarized light curve of a neutron star and its average. We will continue in a subsequent publication with predictions of the net polarization for a realistic model of the emission from the surface of a neutron star.

3.3.1 Polarization light curve of an NS

When an observer measures the polarization of a rotating NS, the amount and angle of polarization will generally vary because the rotation and magnetic axes are usually not aligned together. We define the angular separation between the magnetic and rotational axes as γ. The magnetic inclination angle i ($\equiv\pi/2 - \alpha$) can be related to the inclination above the rotational equator i_r and the rotational phase ϕ between the previous time the two axes coincided in the observer's meridional plane. The relation is

$$\sin i = \sin i_r \cos\gamma + \cos i_r \sin\gamma \cos\phi. \tag{11}$$

If we work in a coordinate system aligned with the rotational z-axis, and a y-axis that is perpendicular to the plane containing the line of sight and the z-axis, then the observer's direction is

$$\hat{\boldsymbol{o}} = \cos i_r \hat{\boldsymbol{x}} + \sin i_r \hat{\boldsymbol{z}}. \tag{12}$$

If we use the rotational phase ϕ and the separation γ between the two axes, the direction of the magnetic axis is

$$\hat{\boldsymbol{m}} = \sin\gamma\cos\phi\hat{\boldsymbol{x}} + \sin\gamma\sin\phi\hat{\boldsymbol{y}} + \cos\gamma\hat{\boldsymbol{z}}. \tag{13}$$

Using these relations, we can calculate the cosine and sine of twice the *apparent* angle ψ that the magnetic axis makes with the y-axis. These are needed if we wish to known the direction of linear polarization. To do so, we project the polarization state $|S_1\rangle$, in which the net polarization will be in (e.g. Section 3.2) on to the polarization states $|S_{O,1}\rangle$ and $|S_{O,2}\rangle$ of the observer. $|S_{O,1}\rangle$ describes linear polarization in the direction of the observer's y-axis and $|S_{O,2}\rangle$ describes polarization in a direction rotated by 45°. The projections are

$$\langle S_{O,1}|S_1\rangle = \cos 2\psi = \frac{2\{[\hat{\boldsymbol{m}} - (\hat{\boldsymbol{m}}\cdot\hat{\boldsymbol{o}})\hat{\boldsymbol{o}}]\cdot\hat{\boldsymbol{y}}\}^2}{|\hat{\boldsymbol{m}} - (\hat{\boldsymbol{m}}\cdot\hat{\boldsymbol{o}})\hat{\boldsymbol{o}}|^2} - 1 \tag{14}$$

$$= \frac{2(\sin\gamma\sin\phi)^2}{1 - (\cos\gamma\sin i_r + \cos i_r\sin\gamma\cos\phi)^2} - 1$$

$$\equiv p_1(\gamma, i_r, \phi), \tag{15}$$

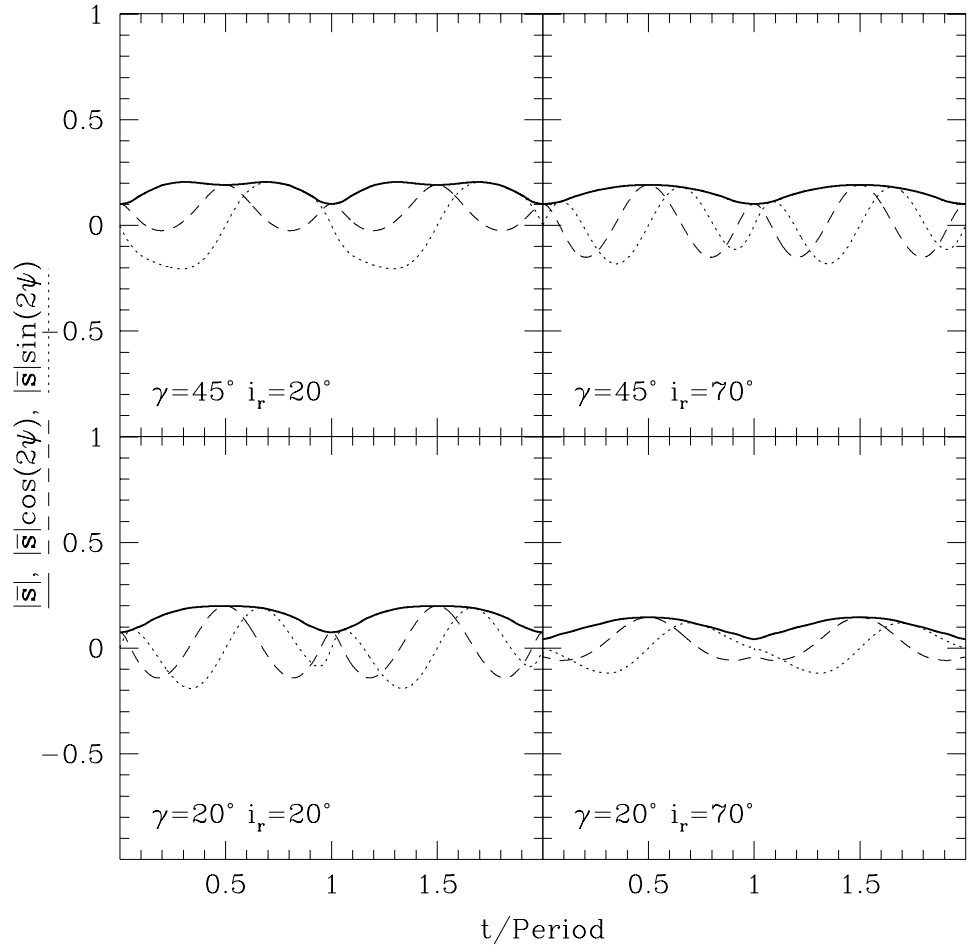

Figure 6. The polarized light curve for $\nu = 0$ Hz and $R = 10$ km (i.e. neglecting the effects that QED has on aligning the polarization). The solid line describes the total linear polarization.

and

$$\langle S_{O,2}|S_1\rangle = \sin 2\psi = \frac{2\{[\hat{\boldsymbol{m}} - (\hat{\boldsymbol{m}}\cdot\hat{\boldsymbol{o}})\hat{\boldsymbol{o}}]\cdot\hat{\boldsymbol{y}}\}\cdot\{[\hat{\boldsymbol{m}} - (\hat{\boldsymbol{m}}\cdot\hat{\boldsymbol{o}})\hat{\boldsymbol{o}}]\cdot\hat{\boldsymbol{x}}\}}{|\hat{\boldsymbol{m}} - (\hat{\boldsymbol{m}}\cdot\hat{\boldsymbol{o}})\hat{\boldsymbol{o}}|^2} \quad (16)$$

$$= \frac{2\sin\gamma\sin i_r\sin\phi(\cos\phi\sin\gamma\sin i_r - \cos\gamma\cos i_r)}{1-(\cos\gamma\sin i_r + \cos i_r\sin\gamma\cos\phi)^2}$$

$$\equiv p_2(\gamma, i_r, \phi). \quad (17)$$

If the total net polarization observed at infinity $|\bar{s}|$ is calculated, the functions $p_{1,2}(\gamma, i_r, \phi)$ can now be used to find the actual polarization that will be measured if our polarizers are aligned with the z-axis or 45° to it, respectively.

Results for the 'polarization light curve' for several frequencies and several NS angles are depicted in Figs 6–8. The solid curve is the total polarization. It could be calculated if the measurement yields both $S_{O,1}$ and $S_{O,2}$. If, however, a polarimeter just measures one axis, and it is aligned with y then its measurements will follow the dashed line. If rotated by 45°, the data will follow the dotted line. Clearly, the best possible measurement is that of the time behaviour of the polarization in two axes that yields the large net polarization $|\bar{S}|$ and the various angles in the system. The latter include the angle separating the axes γ, the observer's inclination above the rotational equator i_r and the direction of the rotational axis in the sky.

3.3.2 Time-averaged polarization of an NS

Although the best polarization measurement possible should be time resolved, often is it hard to do so. It is easier to measure the polarization averaged over the spin period. By looking at Figs 6–8 , we see that if our polarimeter is aligned with the rotational axis, a net polarization signal is obtained though it is typically significantly smaller than the absolute polarization. If the polarimeter is rotated by 45°, symmetry dictates a null average signal.

The average polarization depends on γ, the separation between the axis, and i_r, the inclination above the rotational equator. Although for the general population of NS, the two should not be correlated, this is not the case if we wish to study NSs for which their geometry is already known. NS geometry is known for some pulsars from linear polarization swing measurements in the radio band. Because the objects have to be pulsars with beams passing close to the line of sight, there is a selection effect that chooses objects with only $i_r \sim \pi/2 - \gamma$.

Fig. 9 describes the average expected polarization for the different pulsars for which γ and i_r are known. The data are taken from Mitra & Deshpande (1999). We find that the expected time-averaged polarization for the thermal radiation of 10^{12} G-type pulsars is going to be on average five to seven times larger if QED effects are properly taken into account and the measurement is performed in the optical or X-ray bands. One example is PSR 0656+14, which has a measured thermal spectrum (Pavlov, Welty & Cordova 1997). The

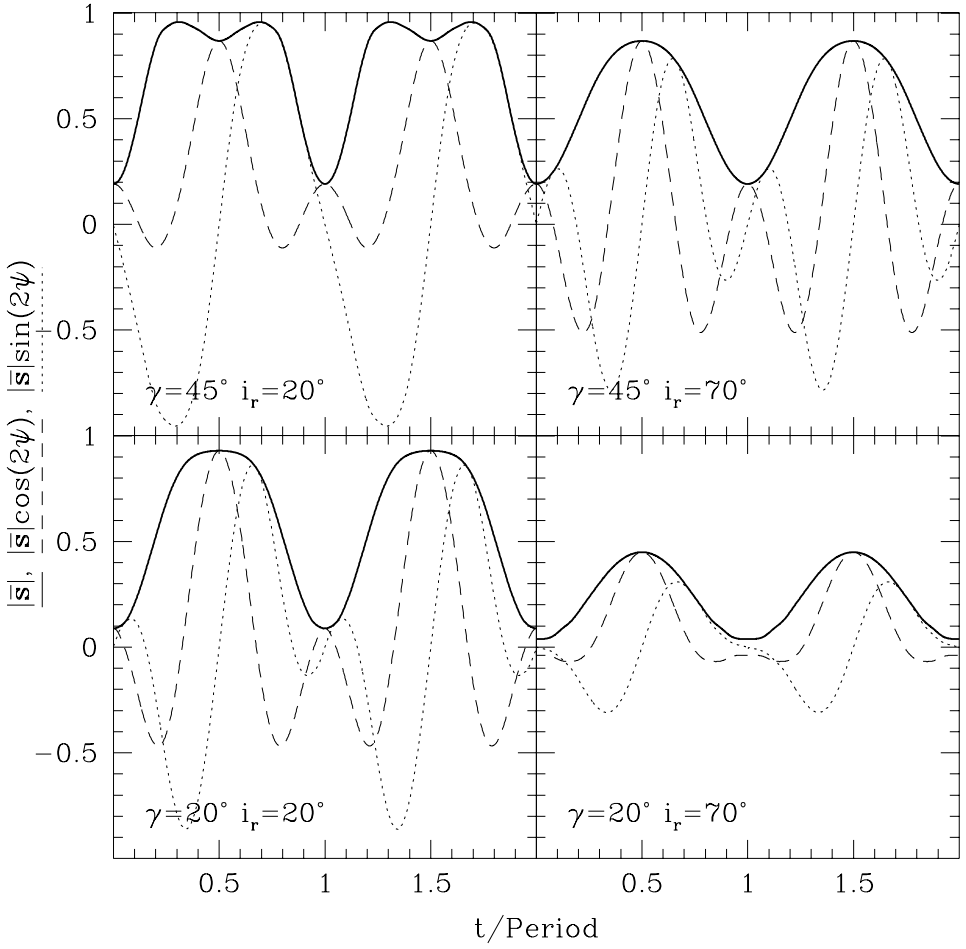

Figure 7. The polarized light curve for $\nu\mu_{30}^2 = 10^{15}$ Hz and $R = 10$ km.

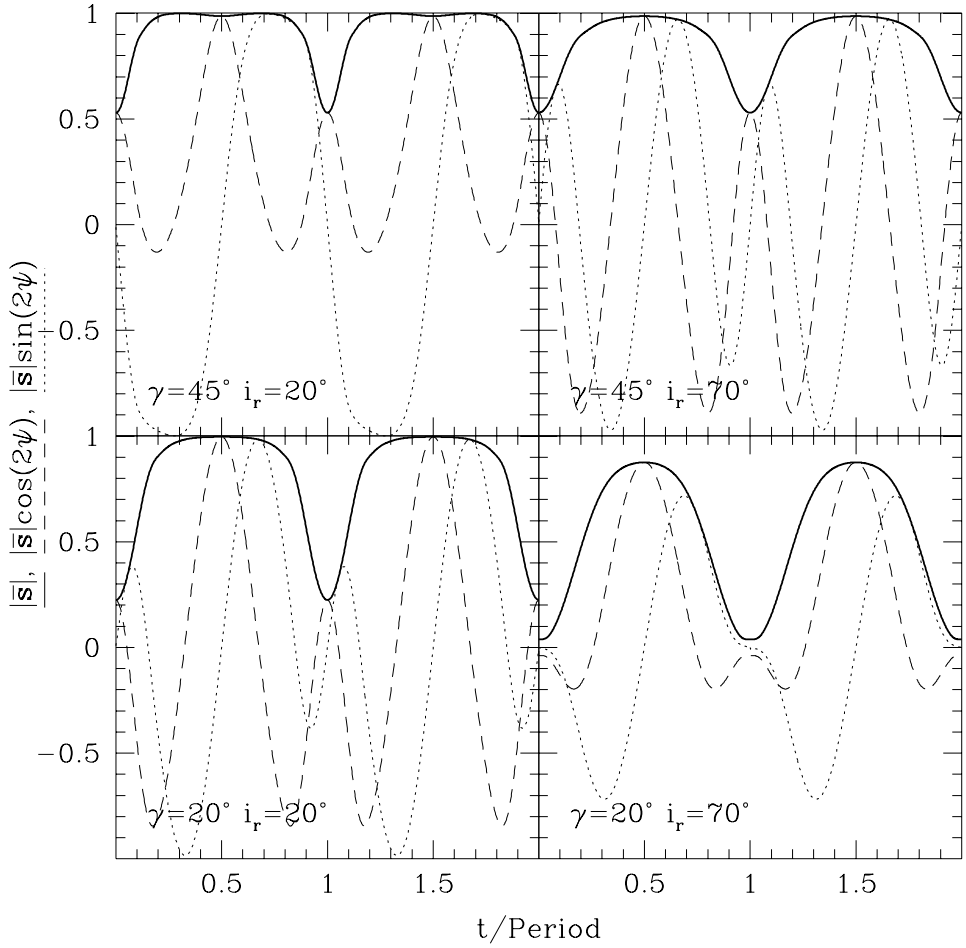

Figure 8. The polarized light curve for $\nu\mu_{30}^2 = 10^{17}$ Hz and $R = 10$ km.

prediction is that the time average of its polarization is going to be approximately 25 per cent times the typical intrinsic polarization of an average surface element. This should be compared with a 5 per cent prediction times the typical average intrinsic polarization, if polarization dragging and aligning does not take place. Note that even if the surface elements were to emit completely polarized radiation, then the maximum possible time-averaged polarization that can be obtained for any geometrical configuration is 12.5 per cent if QED is neglected with typical values being significantly smaller. Thus, the time-averaged measurement of the polarization of PSR 0656+14 is sufficient to prove the effects of QED on aligning the polarization. Because the pulsar was detected in the optical and UV bands, polarimetry can, in principle, already be performed with very long observations.

We must be careful not to overstate the observability of this effect in the optical and near ultraviolet. Typically, if thermal emission from the surface of the star dominates in the optical, the sources are exceptionally faint and would require approximately one night of observing time on a 10-m-class telescope to detect the intrinsic polarization of the source. Furthermore, contamination by non-thermal emission is typically important. For example, even in the optical $\sim$30 per cent of the emission from PSR 0656+14 is non-thermal (Pavlov et al. 1997). Disentangling these two emission mechanisms in the optical is difficult but possible in principle. In the X-rays the signal is much stronger and non-thermal emission plays a lesser role. However, we do not now have instruments measure the polarization of X-ray radiation from astrophysical sources.

4 DISCUSSION AND SUMMARY

It is well known that the intrinsic polarization of the thermal radiation emanating from any NS surface element should be highly polarized. This is a direct result of the effects that the magnetic field has on photon propagation. However, it was thought until recently that because each surface element has a different magnetic field orientation, the combined emission for all the different surface elements would result in a low net polarization for the integrated light. This conclusion, however, rests on the assumption that nothing special happens to the polarization angles along the way. Here, we have shown that QED does have a major effect on the polarization angles in the magnetosphere.

In the presence of QED, the vacuum becomes birefringent. If the differences in the indices of refraction are large enough, 'adiabatic evolution' of the polarization will evolve each polarization state separately by up to a distance $r_{\rm pl}$, the polarization-limiting radius. If the states change slowly because the magnetic field orientation changes, the direction of polarization will change as well. This phenomenon is known to be important for radio waves arising from plasma birefringence (Cheng & Ruderman 1979). The main differences between the two effects are first that plasma birefringence becomes progressively more important for longer wavelengths, as opposed to the shorter wavelengths in which vacuum birefringence becomes progressively more important. Secondly, the amount of actual plasma birefringence is hard to predict accurately, because the amount of plasma present varies according to the pulsar model

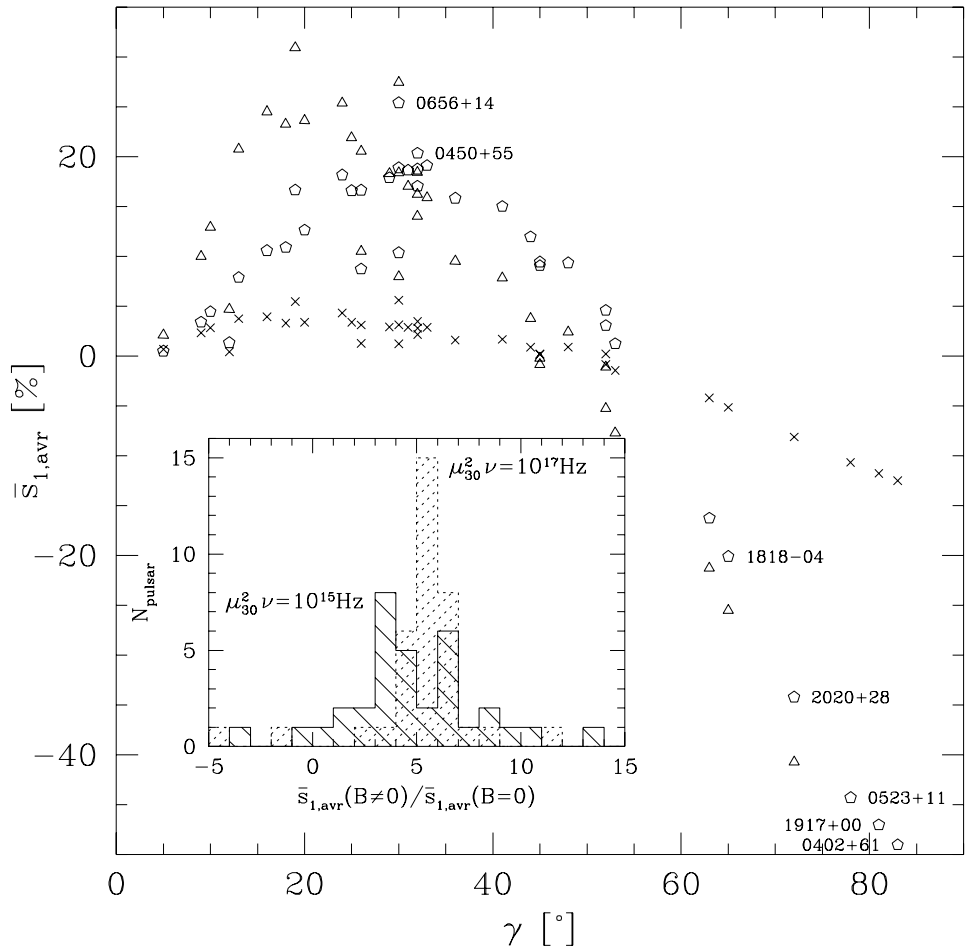

Figure 9. The average linear polarization expected for the thermal radiation of pulsars for which their geometrical angles are known (γ, the separation between the magnetic and rotation axes and i_r, the observer's inclination above the rotational equator). The crosses are the small polarizations expected if polarization dragging is neglected. The triangles and pentagons are the higher polarizations expected for $\nu\mu_{30}^2 = 10^{15}$ and 10^{17} Hz, respectively, when $R = 10$ km (i.e. for optical and X-ray frequencies, for a typical 10^{12} G NS. The inset is a histogram of the increase in average polarization when QED is not neglected.

adopted. Vacuum birefringence depends only on the magnetic field of the NS.

If the polarization limiting radius r_{pl} is far from the surface of the NS, the adiabatic evolution arising from QED birefringence has a very interesting effect – it aligns the polarization angles such that large net polarizations are obtained. The further from the surface that the coupling of the modes takes place (where adiabatic evolution fails), the better is the alignment of rays originating from different surface elements. For typical magnetic fields of 10^{12} G, the alignment is already important for optical and UV photons. And it should be almost complete in X-rays. In stronger fields, as are predicted to exist on magnetars, the alignment should be almost complete even in the optical and the polarization would be very high. This should be compared with the predictions neglecting polarization alignment that always result with significantly lower polarizations.

If the magnetic and rotational axes are misaligned, as is generally the case, the direction of linear polarization changes with the rotation phase. As a result, the time-averaged measurements generally yield smaller net polarizations than time-resolved measurements. The latter are therefore much more preferable. However, they require a more elaborate measuring technique, which for the very faint thermal signal of PSRs is highly non-trivial.

Generally, a circular polarization component along one ray arises when the polarization limiting radius is not orders of magnitude larger than the radius of the NS. This is caused by the fact that while coupling of the states occurs at $r \sim r_{pl}$, the magnetic field is changing its orientation relative to the ray. However, when summed over the image, the circular component vanishes by symmetry. Therefore, any measurement of a non-vanishing circular component in the thermal radiation would imply that the system has broken its symmetry between the apparent sides of the magnetic axis. This can happen, for example, if the magnetic field has a non-symmetric component (rotation, higher multipoles, offset dipole, etc.). It can happen if the temperature (and therefore emission) is not only a function of magnetic latitude (e.g. if there are 'hotspots'). It can also arise because a rotating NS will Doppler boost the radiation from one apparent side of the rotation axis to the blue and the other side to the red. A circular component was also shown to arise when taking the effects that rotation have on the decoupling process itself (Heyl & Shaviv 2000). The main difference between the two types of circular components is that the latter type increases with frequency, while the circular component that arises from asymmetries is largest for optical or UV (for $\sim 10^{12}$ G), when the polarization limiting radius is comparable to the radius of the NS.

Polarization measurements of the thermal radiation will clearly be very beneficial. First, the measurement of polarization will verify the birefringence induced by a magnetic field predicted by QED. Magnetic vacuum birefringence has not yet been detected.

Moreover, measurement of polarization often elucidates the geometry of the systems. In this case, however, it could also give information on actual physical parameters. For example, if the magnetic dipole moment μ is known (e.g. from a spin-down rate measurement) then R can be extracted from the polarization measurement, which indicate how much alignment has taken place. The more alignment is observed, the smaller the radius has to be because the NS apparent solid angle at $r_{\rm pl}$ is then smaller. In AXPs, it could be used to verify their extreme magnetic nature.

ACKNOWLEDGMENTS

Support for this work was provided by the National Aeronautics and Space Administration through *Chandra* Postdoctoral Fellowship Award Number PF0-10015 issued by the *Chandra* X-ray Observatory Centre, which is operated by the Smithsonian Astrophysical Observatory for and on behalf of NASA under contract no NAS8-39073. NS wishes to thank CITA for the fellowship that supported him.

REFERENCES

Bakalov D. et al., 1998, Quant. Semiclass. Opt., 10, 239
Barnard J.J., 1986, ApJ, 303, 280
Cheng A.F., Ruderman M.A., 1979, ApJ, 229, 348
Ginzburg V.L., Ozernoĭ L.M., 1965, Sov. Phys. JETP, 20, 689
Goldreich P., Julian W.H., 1969, ApJ, 157, 869
Heyl J.S., Hernquist L., 1997, J. Phys. A, 30, 6485
Heyl J.S., Shaviv N.J., 2000, MNRAS, 311, 555
Heyl J.S., Shaviv N.J., 2002, Phys. Rev. D, 66, 023002
Iacoponi E., Zavattini E., 1979, Phys. Lett. B, 85, 151
Jackson J.D., 1975, Classical Electrodynamics, 2nd edn. Wiley, New York
Kanno S., 1975, PASJ, 27, 287
Kubo H., Nagata R., 1983, J. Opt. Soc. Am., 73, 1719
Lodenqual J., Canuto V., Ruderman M., Tsuruta S., 1974, ApJ, 190, 141
Meszaros P., Ventura J., 1979, Phys. Rev. D, 19, 3565
Misner C., Thorne K.S., Wheeler J.A., 1973, Gravitation. Freeman, San Francisco
Mitra D., Deshpande A.A., 1999, A&A, 346, 906
Nezrick F., 1999, Nucl. Phys. B, Proc. Suppl., 72, 198
Page D., 1995, ApJ, 442, 273
Pavlov G.G., Shibanov I.A., 1978, A.Zh., 55, 373
Pavlov G.G., Zavlin V.E., 2000, ApJ, 529, 1011
Pavlov G.G., Welty A.D., Cordova F.A., 1997, ApJ, 489, L75
Pineault S., 1977, MNRAS, 179, 691
Rizzo C., 1998, Europhys. Lett., 41, 483
Shaviv N.J., Heyl J.S., Lithwick Y., 1999, MNRAS, 306, 333
Tsai W., Erber T., 1975, Phys. Rev. D, 12, 1132
Ventura J., 1979, Phys. Rev. D, 19, 1684
Ventura J., Nagel W., Meszaros P., 1979, ApJ, 233, L125

This paper has been typeset from a TEX/LATEX file prepared by the author.